“Divide and conquer” semiclassical molecular dynamics: A practical method for spectroscopic calculations of high dimensional molecular systems

Giovanni Di Liberto, Riccardo Conte, and Michele Ceotto

Citation: The Journal of Chemical Physics **148**, 014307 (2018);
View online: https://doi.org/10.1063/1.5010388
View Table of Contents: http://aip.scitation.org/toc/jcp/148/1
Published by the American Institute of Physics

"Divide and conquer" semiclassical molecular dynamics: A practical method for spectroscopic calculations of high dimensional molecular systems

Giovanni Di Liberto, Riccardo Conte, and Michele Ceotto[a)]
Dipartimento di Chimica, Università degli Studi di Milano, Via C. Golgi 19, 20133 Milano, Italy

(Received 25 October 2017; accepted 15 December 2017; published online 4 January 2018)

We extensively describe our recently established "divide-and-conquer" semiclassical method [M. Ceotto, G. Di Liberto, and R. Conte, Phys. Rev. Lett. **119**, 010401 (2017)] and propose a new implementation of it to increase the accuracy of results. The technique permits us to perform spectroscopic calculations of high-dimensional systems by dividing the full-dimensional problem into a set of smaller dimensional ones. The partition procedure, originally based on a dynamical analysis of the Hessian matrix, is here more rigorously achieved through a hierarchical subspace-separation criterion based on Liouville's theorem. Comparisons of calculated vibrational frequencies to exact quantum ones for a set of molecules including benzene show that the new implementation performs better than the original one and that, on average, the loss in accuracy with respect to full-dimensional semiclassical calculations is reduced to only 10 wavenumbers. Furthermore, by investigating the challenging Zundel cation, we also demonstrate that the "divide-and-conquer" approach allows us to deal with complex strongly anharmonic molecular systems. Overall the method very much helps the assignment and physical interpretation of experimental IR spectra by providing accurate vibrational fundamentals and overtones decomposed into reduced dimensionality spectra. *Published by AIP Publishing.*
https://doi.org/10.1063/1.5010388

I. INTRODUCTION

The simulation of vibrational spectra of high-dimensional systems is an important open issue in quantum mechanics. The challenge is to beat the curse of dimensionality that plagues any quantum method in both electronic and nuclear spectroscopy simulations. In fact, the exact treatment of quantum problems often implies the setup of a grid. As a consequence, the computational cost scales exponentially with dimensionality, and only simulations involving a few atoms can be exactly performed.[1–5] Alternatively, perturbative quantum methods have also been successfully applied to many systems, but they are intrinsically limited to a single reference geometry.[6–11] High-dimensional systems, such as peptides, are instead usually simulated through *ad hoc* scaled harmonic approaches or by means of classical mechanics, either using force fields[12–14] or employing *ab initio* molecular dynamics (AIMD)[15–21] approaches in which the nuclear forces are calculated using electronic structure codes. In classical simulations, the curse of dimensionality is significantly tamed with respect to quantum mechanical counterparts. However, a purely classical dynamics simulation is unable to describe tunneling effects, zero point energies (ZPEs), overtones, and other important spectroscopic quantum features.

Semiclassical dynamics employs classical trajectories to reproduce quantum mechanical effects. In semiclassical methods, spectra are calculated in a time-dependent way, i.e., by Fourier transforming the survival amplitude or the autocorrelation function of some observables (such as the dipole moment).[22] Semiclassical methods based on the coherent states Herman-Kluk propagator[23–29] and the initial value representation [semiclassical initial value representation (SCIVR)][30–32] are robust, have been proven to reproduce quantum effects quite quantitatively,[22,33–56] and have been shown to have an accuracy in spectra calculations often within 1% of exact results.[35,57] Recently, the multiple-coherent (MC)-SCIVR technique has been developed. It allows us to perform on-the-fly semiclassical molecular dynamics simulations given a few input trajectories.[58–65] The approach is amenable to *ab initio* direct molecular dynamics, thus avoiding the effort to construct an accurate analytical potential energy surface (PES) which may be quite demanding especially for large systems[66–74] and permits to faithfully reproduce quantum effects like quantum resonances,[60] intra-molecular and long-range dipole splittings, and the quantum resonant ammonia umbrella inversion.[62] Nevertheless, all SCIVR methods run out of steam when straightforwardly applied to problems involving large-sized systems.

Understanding the reasons of such a limitation is the first step to do for dealing with the curse of dimensionality and possibly overcoming it. The semiclassical wavepacket for a system of N degrees of freedom (DOFs) consists in the direct product of N monodimensional (Gaussian) wavefunctions $|\Psi(t)\rangle = |\psi_1(t)\rangle \ldots |\psi_N(t)\rangle$. When the time-dependent overlap $\langle\Psi(0)|\Psi(t)\rangle$ is Fourier transformed to generate the spectrum, the simulation time should have been long enough to provide a significant overlap. In other words, if the trajectory does not periodically return to the surroundings of the phase-space region where it started, a noisy signal will be

a)Author to whom correspondence should be addressed: michele.ceotto@unimi.it

collected. If, instead, the multidimensional classical trajectory is such that $(\mathbf{p}(t), \mathbf{q}(t))$ approaches several times $(\mathbf{p}(0), \mathbf{q}(0))$, then the overlap $\langle\Psi(0)|\Psi(t)\rangle$ is sizable and the signal associated with the vibrational features will prevail on the noise. The curse of dimensionality occurs because each monodimensional coherent state overlap $\langle\psi_i(0)|\psi_i(t)\rangle$ should be significant for *all* dimensions at the same time. Even for uncoupled oscillators with non-commensurable frequencies, the concomitant overlapping event is rarer and rarer as the dimensionality increases, and the simulation time has to be much prolonged.[58] The present "*divide et impera*" idea starts from the consideration that a full-dimensional classical trajectory, once projected onto a sub-dimensional space, is more likely to provide a useful spectroscopic signal and a clear spectroscopic signal can be obtained in a much shorter amount of time with respect to the full-dimensional case, as we have recently shown.[75] Thus, according to this divide-and-conquer strategy, after dividing the full-dimensional space into mutual disjoint subspaces, a semiclassical spectroscopic calculation is performed separately for each subspace. While the classical trajectories are full-dimensional, the semiclassical calculations employ subspace information for calculating each partial spectrum. Composition of the projected spectra provides the full-dimensional one. Considering that nuclear spectra of high-dimensional systems are often too crowded for an unambiguous interpretation, this "divide-and-conquer" strategy will also allow us to better read and understand the physics behind the spectra and help the interpretation of experimental results.

In this paper, we introduce some new features that significantly enhance the accuracy of our divide-and-conquer semiclassical initial value representation (DC-SCIVR) method. Accuracy of results is estimated by comparison to exact values for systems up to 30 degrees of freedom (DOFs). In Sec. II, we first recall the basics of time averaged semiclassical spectral density calculations,[76,77] and then we describe in details the DC-SCIVR approach and two new subspace-separation criteria. In Sec. III, we test the performance of DC-SCIVR on strongly coupled Morse oscillators, real molecular systems like H_2O, CH_2O, CH_4, and CH_2D_2, the very challenging Zundel cation ($H_5O_2^+$), and, finally, the benzene molecule which is, at the best of our knowledge, the highest dimensional molecular system for which exact quantum vibrational calculations have been performed.[78] A summary and some conclusions end the paper.

II. A DIVIDE-AND-CONQUER STRATEGY FOR SEMICLASSICAL DYNAMICS

This section recalls the derivation of the DC-SCIVR expression for spectroscopic calculations. We start from the SCIVR power spectrum formulation and its multiple coherent state time averaging implementation (MC-SCIVR) and then move to the "divide-and-conquer" working formula. Finally, we present three different techniques for partitioning the full-dimensional vibrational space into suitable lower-dimensional subspaces.[75]

A. The SCIVR time averaged spectral density

We start by writing the power spectrum $\mathrm{I}(E)$ of a molecular system, characterized by the Hamiltonian $\hat{H}$, as the Fourier transform of the survival amplitude[22] of a given and arbitrary reference state $|\chi\rangle$,

$$\mathrm{I}(E) \equiv \frac{1}{2\pi\hbar}\int_{-\infty}^{+\infty}\left\langle\chi\left|e^{-i\hat{H}t/\hbar}\right|\chi\right\rangle e^{iEt/\hbar}dt. \tag{1}$$

In semiclassical (SC) molecular dynamics, the quantum time-evolution operator $e^{-i\hat{H}t/\hbar}$ of Eq. (1) is substituted by the stationary-phase approximation to its Feynman path integral representation.[79] In the position representation, the semiclassical propagator is a matrix whose elements are obtained as products of a complex action exponential and a stationary-phase pre-exponential factor, summed over all classical trajectories that connect the two endpoints.[41,80–88] The search for these trajectories is hampered by the rigid double-boundary condition. In the SCIVR dynamics, introduced by Miller and later also developed by Heller, Herman, Kluk, and Kay,[22,27,28,30,31,34,57,89] the propagator is instead formulated in terms of classical trajectories determined by initial conditions $(\mathbf{p}(0), \mathbf{q}(0))$ so that Eq. (1) becomes

$$\left\langle\chi\left|e^{-i\hat{H}t/\hbar}\right|\chi\right\rangle \approx \left(\frac{1}{2\pi\hbar}\right)^F \iint d\mathbf{p}(0)\, d\mathbf{q}(0)$$
$$C_t(\mathbf{p}(0), \mathbf{q}(0))\, e^{\frac{i}{\hbar}S_t(\mathbf{p}(0),\mathbf{q}(0))}\langle\chi\,|\mathbf{p}(t)\,\mathbf{q}(t)\rangle\,\langle\mathbf{p}(0)\,\mathbf{q}(0)|\,\chi\rangle, \tag{2}$$

where F is the number of degrees of freedom, $S_t(\mathbf{p}(0), \mathbf{q}(0))$ is the classical action, and $C_t(\mathbf{p}(0), \mathbf{q}(0))$ indicates the pre-exponential stationary-phase factor. If $|\mathbf{p}(t), \mathbf{q}(t)\rangle$ is represented as a coherent state[22,89–91] of the type

$$\langle\mathbf{x}|\mathbf{p}(t), \mathbf{q}(t)\rangle = \left(\frac{\det(\Gamma)}{\pi^F}\right)^{1/4} e^{-(\mathbf{x}-\mathbf{q}(t))^T\Gamma(\mathbf{x}-\mathbf{q}(t))/2+i\mathbf{p}^T(t)(\mathbf{x}-\mathbf{q}(t))/\hbar}, \tag{3}$$

where Γ is a diagonal width matrix with coefficients usually equal to the square root of the vibrational frequencies for bound states calculations, then the pre-exponential factor becomes

$$C_t(\mathbf{p}(0), \mathbf{q}(0)) = \sqrt{\det\left|\frac{1}{2}\left(\frac{\partial\mathbf{q}(t)}{\partial\mathbf{q}(0)} + \frac{\partial\mathbf{p}(t)}{\partial\mathbf{p}(0)} - i\hbar\Gamma\frac{\partial\mathbf{q}(t)}{\partial\mathbf{p}(0)} + \frac{i}{\Gamma\hbar}\frac{\partial\mathbf{p}(t)}{\partial\mathbf{q}(0)}\right)\right|}, \tag{4}$$

and Eq. (2) is commonly known as the Herman-Kluk survival amplitude of the Hamiltonian $\hat{H}$. However, for complex systems, the phase-space integration of Eq. (2) requires too many trajectories to be feasible. To overcome this limitation, Miller and

Kaledin introduced a time averaged version of the semiclassical propagator (TA-SCIVR),[76,77] which significantly reduces the computational overhead

$$\mathrm{I}(E) = \frac{1}{(2\pi\hbar)^F} \iint d\mathbf{q}(0)\, d\mathbf{p}(0)\, \frac{\mathrm{Re}}{\pi\hbar T} \int_0^T dt_1 \int_{t_1}^{+\infty} dt_2 e^{i\left(S_{t_2}(\mathbf{p}(0),\mathbf{q}(0))+Et_2\right)/\hbar} \langle\chi|\mathbf{p}(t_2),\mathbf{q}(t_2)\rangle e^{-i\left(S_{t_1}(\mathbf{p}(0),\mathbf{q}(0))+Et_1\right)/\hbar} \times \langle\mathbf{p}(t_1),\mathbf{q}(t_1)|\chi\rangle C_{t_2}(\mathbf{p}(t_1),\mathbf{q}(t_1)), \tag{5}$$

where t_1 is the additional time averaging variable and t_2 is the original Fourier transform variable. In Eq. (5), the integrand is time averaged by taking into account different portions of time length $t_2 - t_1$ of the same trajectory started in $(\mathbf{p}(0), \mathbf{q}(0))$. Considering that the pre-exponential factor is of the type $e^{i\omega t}$ for a harmonic ω-frequency system, Eq. (4) can be reasonably approximated as $C_t(\mathbf{p}(0), \mathbf{q}(0)) = e^{i\phi_t}$, where $\phi_t = \text{phase}\left[C_t(\mathbf{p}(0), \mathbf{q}(0))\right]$, leading to the computationally more convenient separable approximation version of TA-SCIVR,[76,77]

$$\mathrm{I}(E) = \left(\frac{1}{2\pi\hbar}\right)^F \iint d\mathbf{p}(0)\, d\mathbf{q}(0)\, \frac{1}{2\pi\hbar T} \times \left| \int_0^T e^{\frac{i}{\hbar}\left[S_t(\mathbf{p}(0),\mathbf{q}(0))+Et+\phi_t\right]} \langle\chi|\mathbf{p}(t),\mathbf{q}(t)\rangle dt \right|^2. \tag{6}$$

Equation (6) is more amenable than (5) to the phase-space Monte Carlo integration, given the positive-definite integrand, and it has been tested with excellent results on several molecular systems. However, TA-SCIVR still requires thousands of trajectories per degree of freedom to reach convergence.[76,77,92,93] To further reduce the computational effort, the multiple-coherent time averaged SCIVR (MC-SCIVR) has been introduced.[58–62,94] In the MC-SCIVR formulation, the reference state $|\chi\rangle$ is written as a combination of coherent states placed at the classical phase-space points $\left(\mathbf{p}^i_{\mathrm{eq}}, \mathbf{q}^i_{\mathrm{eq}}\right)$, i.e., $|\chi\rangle = \sum_{i=1}^{N_{\mathrm{states}}} \left|\mathbf{p}^i_{\mathrm{eq}}, \mathbf{q}^i_{\mathrm{eq}}\right\rangle$. $\mathbf{q}^i_{\mathrm{eq}}$ is an equilibrium position, while $\mathbf{p}^i_{\mathrm{eq}}$ is obtained in a harmonic fashion as $\left(p^i_{j,\mathrm{eq}}\right)^2/2m = \hbar\omega_j\left(n + 1/2\right)$, where j is a generic normal mode, ω_j is the associated harmonic frequency, and m is unitary in mass-scaled normal mode coordinates. Equation (6) has been shown to be quite accurate with respect to exact quantum mechanical simulations for the several molecules tested, even when applied to systems as complex as glycine.[62,63,92,93]

B. The "divide-and-conquer" strategy applied to semiclassical dynamics

In this section, we provide a more detailed explanation of the "divide-and-conquer" strategy previously introduced elsewhere.[75] The idea is to calculate the power spectrum $\mathrm{I}(E)$ of Eq. (1) as composition of partial spectra $\widetilde{\mathrm{I}}(E)$ each one calculated in a reduced M-dimensional phase space $(\tilde{\mathbf{p}}, \tilde{\mathbf{q}})$ of the full N_{vib}-dimensional space $(\mathbf{p}, \mathbf{q})$ $\equiv$ $(p_1, q_1, \ldots, \tilde{p}_{i+1}, \tilde{q}_{i+1}, \ldots, \tilde{p}_{i+M}, \tilde{q}_{i+M}, \ldots, p_{N_{vib}}, q_{N_{vib}})$. In quantum mechanics, where operators can be represented by matrices, the projection of an operator onto a sub-space is obtained by a preliminary suitable singular-value decomposition (SVD),[95] followed by a subsequent matrix multiplication between the full-dimensional operator and the projector. Semiclassically operators are represented in phase-space coordinates and a suitable SVD is the one involving the displacement matrix $\mathbf{D}$ for the M-dimensional subspace.[95,96] In our case, $\mathbf{D}$ is a $\mathrm{N}_{\mathrm{vib}} \times \mathrm{M}$ dimensional matrix and a singular-value decomposition is obtained when $\mathbf{D} = \mathbf{U}\boldsymbol{\Sigma}\mathbf{V}$, where $\mathbf{U}$ is a $\mathrm{N}_{\mathrm{vib}} \times \mathrm{M}$ matrix, Σ is a $\mathrm{M} \times \mathrm{M}$ one, and V is a $\mathrm{M} \times \mathrm{M}$ one. The matrix $\Delta = \mathbf{U}\mathbf{U}^T$ is the projector onto the M-dimensional subspace. Eventually, any matrix $\mathbf{A}$ is projected onto the reduced M-dimensional subspace by taking $\tilde{\mathbf{A}} = \boldsymbol{\Delta}\mathbf{A}\boldsymbol{\Delta}$ and retaining the $\mathrm{M} \times \mathrm{M}$ sub-block of non-zero elements. Similarly, any vector $\mathbf{q}$ is projected by taking $\tilde{\mathbf{q}} = \boldsymbol{\Delta}\mathbf{q}$. Given these considerations, the projected power spectrum can be written as

$$\widetilde{I}(E) = \left(\frac{1}{2\pi\hbar}\right)^M \iint d\tilde{\mathbf{p}}(0)\, d\tilde{\mathbf{q}}(0)\, \frac{1}{2\pi\hbar T} \times \left| \int_0^T e^{\frac{i}{\hbar}\left[\tilde{S}_t(\tilde{\mathbf{p}}(0),\tilde{\mathbf{q}}(0))+Et+\tilde{\phi}_t\right]} \langle\tilde{\chi}|\tilde{\mathbf{p}}(t),\tilde{\mathbf{q}}(t)\rangle dt \right|^2, \tag{7}$$

where the M-dimensional coherent state in the M-dimensional sub-space is

$$\langle\tilde{\mathbf{x}}|\tilde{\mathbf{p}}(\mathbf{t}),\tilde{\mathbf{q}}(\mathbf{t})\rangle = \left(\frac{\det(\tilde{\Gamma})}{\pi^M}\right)^{\frac{1}{4}} e^{-(\tilde{\mathbf{x}}-\tilde{\mathbf{q}}(t))^T\tilde{\mathbf{\Gamma}}(\tilde{\mathbf{x}}-\tilde{\mathbf{q}}(t))/2+i\tilde{\mathbf{p}}^T(t)(\tilde{\mathbf{x}}-\tilde{\mathbf{q}}(t))/\hbar}, \tag{8}$$

where the matrix $\tilde{\Gamma} = \mathbf{U}\mathbf{U}^T\Gamma\mathbf{U}^T\mathbf{U}$ is the projected Gaussian width matrix. $\langle\tilde{\mathbf{x}}|\tilde{\chi}\rangle$ is obtained in a similar way. The phase-space integration is now limited to $\int\int d\tilde{\mathbf{p}}(0)\, d\tilde{\mathbf{q}}(0)$, i.e., a 2M-dimensional space. This greatly reduces the computational cost and the number of trajectories necessary to converge the Monte Carlo integration. Furthermore, the sampling of the initial conditions of the full-dimensional trajectories can be done according to a Husimi distribution in the subspace with the external degrees of freedom at equilibrium. The representation of the phase $\tilde{\phi}_t$ in reduced dimensionality is approximated as $\tilde{\phi}_t = \text{phase}\left[\tilde{C}_t(\tilde{\mathbf{p}}(0), \tilde{\mathbf{q}}(0))\right]$, where the pre-exponential factor is calculated according to Eq. (4) and each matrix block is of the type $\partial\tilde{\boldsymbol{q}}(t)/\partial\tilde{\boldsymbol{q}}(0)$, and so on. The only component of Eq. (7) that cannot be projected onto the sub-space using the SVD is the classical action

$$\tilde{S}_t(\tilde{\mathbf{p}}(0), \tilde{\mathbf{q}}(0)) = \int_0^T \left[\frac{1}{2}m\dot{\tilde{\mathbf{q}}}^2(t) + V_S(\tilde{\boldsymbol{q}}(t))\right] dt \tag{9}$$

since the expression of the "projected" potential $V_S(\tilde{\boldsymbol{q}}(t))$ cannot be directly obtained. More specifically, the projected

potential $V_S(\tilde{\boldsymbol{q}}(t))$ should be the potential such that an M-dimensional trajectory starting with initial conditions $(\tilde{\mathbf{p}}(0), \tilde{\mathbf{q}}(0))$ visits at all times t the same phase-space points $(\tilde{\mathbf{p}}(t), \tilde{\mathbf{q}}(t))$ obtained upon projection of the full-dimensional trajectory. However, the potential $V_S(\tilde{\boldsymbol{q}}(t))$ is known only for systems characterized by a separable potential. In an effort to find a general and suitable expression for $V_S(\tilde{\boldsymbol{q}}(t))$, we notice that the full-dimensional trajectory is continuous with continuous first derivatives for the full-dimensional molecular potential $V(\boldsymbol{q}(t))$, and we deduce that the M-dimensional trajectory and $V_S(\tilde{\mathbf{q}}(t))$ have the same features. In a straightforward way, we initially define the sub-dimensional potential as

$$V_S(\tilde{\mathbf{q}}(t)) \equiv V\left(\tilde{\mathbf{q}}(t); \mathbf{q}_{N_{vib}-M}(t)\right), \tag{10}$$

where the positions $\mathbf{q}_{N_{vib}-M}(t)$ belonging to the other subspaces have been downgraded to parameters. Then, we introduce a time-dependent field such that

$$V_S(\tilde{\mathbf{q}}(t)) = V\left(\tilde{\mathbf{q}}(t); \mathbf{q}^{eq}_{N_{vib}-M}\right) + \lambda(t) \tag{11}$$

since it is more intuitive and convenient to represent the reduced dimensionality potential in terms of the conditioned full-dimensional one (with the parametric coordinates in their equilibrium positions) plus an external time-dependent field. In agreement with our previous work,[75] we take the following expression for $\lambda(t)$:

$$\lambda(t) = V\left(\tilde{\mathbf{q}}(t); \mathbf{q}_{N_{vib}-M}(t)\right) - \left[V\left(\tilde{\mathbf{q}}(t); \mathbf{q}^{eq}_{N_{vib}-M}\right) + V\left(\mathbf{q}^{eq}_{M}; \mathbf{q}_{N_{vib}-M}(t)\right)\right] \tag{12}$$

which is exact in the separable limit. To verify this, we consider for simplicity a two-dimensional separable potential of the type $V(q_1(t), q_2(t)) = V_1(q_1(t)) + V_2(q_2(t))$ but the procedure is readily generalizable to separable potentials of any dimensionality. In the 2D case, using Eqs. (11) and (12), we obtain $V_S(q_1(t)) = V_1(q_1(t)) - V_1\left(q_1^{eq}\right)$ which is exact. We also notice that in Eq. (12) an additional last term (the value of the instantaneous full-dimensional potential with the subspace coordinates at equilibrium) has been introduced with respect to Eq. (10). It provides a linear term in the action and consequently shifts the spectrum by a constant, allowing us to match on the same scale each partial spectrum $\tilde{\mathrm{I}}(E)$ and to obtain the full-dimensional spectrum $\mathrm{I}(E)$ as a composition of the several $\tilde{\mathrm{I}}(E)$. In this last aspect, the DC-SCIVR procedure is somewhat similar to the one employed by Wehrle, Šulc, and Vaníček in their reduced-dimensionality emission spectra simulations.[97] There, they exploited conservation of energy to derive a projected Lagrangian whose potential energy was made only of a constant term that had the effect to shift the total spectra. Finally, the full-dimensional DC-SCIVR zero point energy (ZPE) can simply be regained by summing up the partial ZPE contributions of each subspace.

To test the effectiveness of our scheme for $V_S(\tilde{\mathbf{q}}(t))$, we consider two strongly coupled monodimensional Morse oscillators, whose analytical potential will be explicitly reported in Sec. III A. Figure 1 reports in the left panel the phase-space plots for a classical trajectory with energy equal to that of the ground state. The black continuous line is for the $(\tilde{\mathbf{p}}(t), \tilde{\mathbf{q}}(t))$ values obtained from the full-dimensional vector which becomes $(\mathbf{p}(t), \mathbf{q}(t)) \equiv (p_1(t), q_1(t), p_2(t), q_2(t))$ in this specific case, evolved according to the full-dimensional potential $V(\boldsymbol{q}(t))$. The green dashed line is for the classical trajectory starting at $(\tilde{\mathbf{p}}(0), \tilde{\mathbf{q}}(0))$ and evolved according to the approximate potential $V_S(\tilde{\mathbf{q}}(t)) = V\left(\tilde{\mathbf{q}}(t); \mathbf{q}^{eq}_{N_{vib}-M}\right)$, i.e., without any $\lambda(t)$ correction. Such a potential is really unfit to describe the projected trajectory motion, since the green curve diverges after a few time steps, as it were describing an unbound system. Two different phase-space plots for the same Morse oscillators appear on the right panel of Fig. 1. Again, the black continuous line is for the exact projected trajectory, while the red dashed line is for the classical trajectory starting at $(\tilde{\mathbf{p}}(0), \tilde{\mathbf{q}}(0))$ and evolved according to the approximate potential $V_S(\tilde{\mathbf{q}}(t))$ of Eq. (11). In this case, the trajectory phase-space plot is typical of a bound system. For one of the two dimensions, the phase-space exact and approximate trajectories can be hardly distinguished. For the other degree of freedom, despite a phase accumulation, the frequency of the approximate trajectory motion is very similar to the exact one.

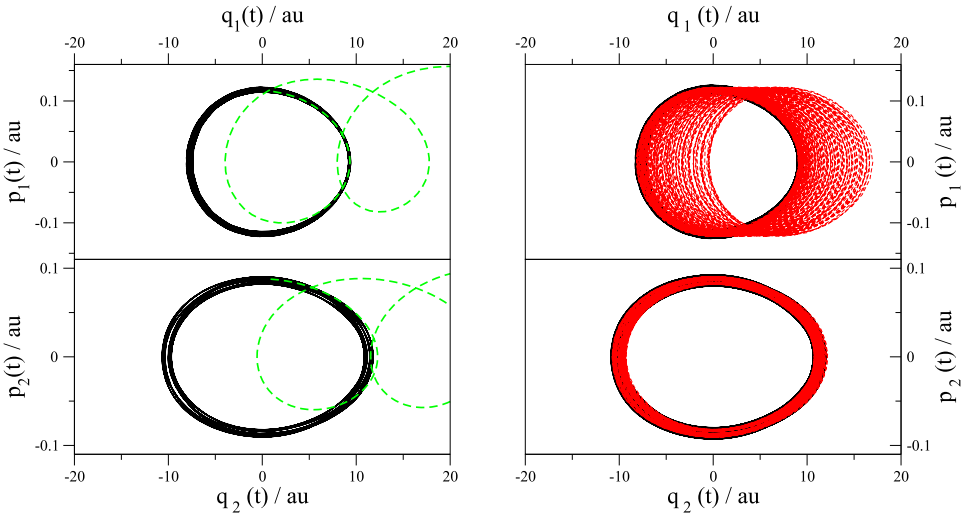

FIG. 1. Mass-scaled phase space plot for the two strongly coupled Morse oscillators of Eq. (18). Left panel: Black continuous lines for the exact and green dashed lines for the potential $V_S(\tilde{\mathbf{q}}(t)) = V\left(\tilde{\mathbf{q}}(t); \mathbf{q}^{eq}_{N_{vib}-M}\right)$. Right panel: Black continuous lines for the exact and red dashed line for the potential of Eq. (11).

C. Vibrational space decomposition into mutually disjoint subspaces

It is now important to define an appropriate strategy for the decomposition of the full-dimensional space into mutually disjoint and convenient subspaces. The identification of relevant DOFs for spectroscopic calculations is a long-standing issue in spectroscopy, and several techniques to determine the "effective modes" have been proposed.[98,99] We present here three possible strategies: one is based on the time evolution of the Hessian matrix and the other two on the evolution of the monodromy matrix. In all cases, a preliminary test trajectory is classically evolved starting from the atomic equilibrium positions and with initial kinetic energy equal to the harmonic zero point energy (ZPE) and distributed among the vibrational modes proportionally to their harmonic frequencies.

1. The Hessian space-decomposition method

We recall a decomposition strategy that has been recently presented[75] for the computation of molecular vibrational spectra. The full mass-scaled Hessian matrix is calculated at each time step and the time averaged value of each Hessian matrix element is obtained, i.e., $\bar{H}_{ij} = \sum_{k=1}^{N} H_{ij}(t_k)/N$, with N the number of time steps. If $|\bar{H}_{ij}| \geq \epsilon$, where ϵ is an arbitrarily fixed threshold parameter, then the degrees of freedom i and j are considered as belonging to the same subspace. If $|\bar{H}_{ij}| < \epsilon$, then i and j can still belong to the same subspace if there exists a third degree of freedom k such that $\bar{H}_{ik}$ and $\bar{H}_{jk}$ are bigger than ϵ. In that case, i and j (and also k) are collected into the same subspace. In Fig. 2, we report how the division into subspaces is affected by the chosen value of ϵ. Clearly for $\epsilon = 0$, all degrees of freedom are on the same full-dimensional space as shown in Fig. 2(a). By gradually increasing the value of ϵ, the subspaces become more and more fragmented as illustrated in Figs. 2(b) and 2(c). Finally, for ϵ bigger than a certain value, the full-dimensional space is broken down into a direct sum of mono-dimensional subspaces, as in Fig. 2(d). In our simulations we usually choose a value of ϵ such that it maximizes the dimensionality of the biggest subspace provided that a spectroscopic signal can be collected and the curse of dimensionality does not kick in. This strategy is very advantageous in terms of computational effort, since the partition of the degrees of freedom into subspaces is instantaneous after the classical trajectory is run and the Hessian matrices calculated. However, there is no evidence that this strategy makes the partial spectra $\widetilde{\mathrm{I}}(E)$ of Eq. (7) the most accurate with respect to the full-dimensional spectrum $\mathrm{I}(E)$ of Eq. (6).

2. Wehrle-Šulc-Vaníček (WSV) space-decomposition method

An alternative decomposition approach (still based on dynamically averaged quantities and an arbitrary threshold) has been recently introduced by Vaníček and co-workers.[97] In fact, to quantify the coupling between various DOFs still in a dynamical way, one can utilize the stability matrix. This is a $2N_{vib}$ dimensional matrix also known as monodromy matrix and defined as

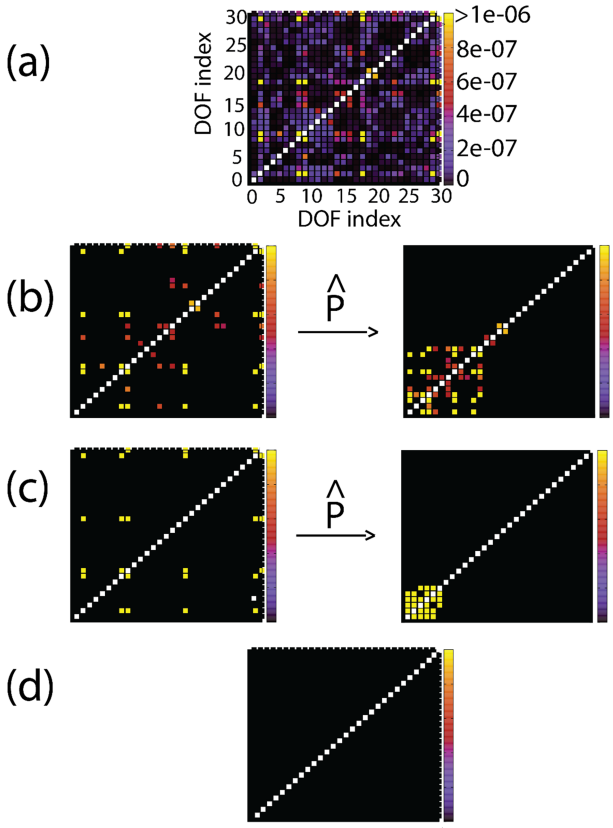

FIG. 2. Hessian matrix elements for a system of 30 degrees of freedom (benzene) greater than a given threshold value ϵ. The greater the value of ϵ, the less dense is the matrix. Diagonal elements are out of scale and are reported as white pixels. Panel (a) shows as pixels only the coupling elements that are greater than $\epsilon = 0$ a.u. Panels (b)–(d) are similar, respectively, for $\epsilon = 4.5\cdot10^{-7}$a.u., $\epsilon = 9\cdot10^{-7}$a.u., and $\epsilon = 6\cdot10^{-6}$a.u. In (b) and (c), the matrix elements have been conveniently arranged after permutations ($\hat{\mathbf{P}}$) into sub-blocks. Each sub-block determines a subspace.

$$\boldsymbol{M}(t) \equiv \begin{pmatrix} \partial \boldsymbol{p}(t)/\partial \boldsymbol{p}(0) & \partial \boldsymbol{p}(t)/\partial \boldsymbol{q}(0) \\ \partial \boldsymbol{q}(t)/\partial \boldsymbol{p}(0) & \partial \boldsymbol{q}(t)/\partial \boldsymbol{q}(0) \end{pmatrix} = \begin{pmatrix} \boldsymbol{M}_{\boldsymbol{pp}} & \boldsymbol{M}_{\boldsymbol{pq}} \\ \boldsymbol{M}_{\boldsymbol{qp}} & \boldsymbol{M}_{\boldsymbol{qq}} \end{pmatrix}. \tag{13}$$

It may be employed to measure how the classical energy is exchanged in time between the DOFs and, by virtue of Liouville's theorem, its determinant is always equal to 1.

In their paper, Vaníček and co-workers define the following quantity **B** to measure the amount of coupling between the vibrational degrees of freedom in a dynamical fashion,

$$B_{ij} = \left|\frac{\beta_{ij}}{\beta_{ii}}\right|,$$
$$\beta_{ij} = \frac{1}{T}\int_0^T dt\,\left(|M_{q_iq_j}(t)| + |M_{q_ip_j}(t)| + |M_{p_iq_j}(t)| + |M_{p_ip_j}(t)|\right), \tag{14}$$

where $|M_{ij}(t)|$ are the absolute values of the monodromy matrix elements of Eq. (13). After an arbitrary parameter ϵ_B is chosen, if the test $max\{B_{ij}, B_{ji}\} \geq \epsilon_B$ is passed, then modes i and j go into the same subspace, following a procedure very similar to the one employed for our Hessian criterion but with the difference that more than a single threshold is used. In our calculations with the WSV method, given an N_{vib} vibrational space, the bigger M-dimensional subspace is determined through a fixed value of ϵ_B. For the remaining $N_{vib} - M$ DOFs,

a different value of ϵ_B is chosen to obtain the biggest subspace between the remaining DOFs and so on and so forth until all DOFs are grouped.

One might wonder if other dynamical quantities fit in the same general scheme made of a trajectory average followed by a comparison versus a threshold value. In this regard, the interested reader may find tests and a thorough discussion of several ways to define $\mathbf{B}$ on the basis of alternative averaged quantities (like, for instance, the correlation matrix of the wavepacket) in Wehrle's doctoral thesis.[100]

3. Jacobi space-decomposition method

We here introduce a new approach to determine a subspace partition which leads to a more accurate calculation of $\widetilde{\mathrm{I}}(E)$. Since in DC-SCIVR the coherent state overlap $\langle\chi|\mathbf{p}(t),\mathbf{q}(t)\rangle$ is already written in terms of direct mono-dimensional overlaps and the action $\tilde{S}_t(\tilde{\mathbf{p}}(0),\tilde{\mathbf{q}}(0))$ is approximated according to Eqs. (9), (11), and (12), the best strategy is one that minimizes the error in decomposing the full-dimensional pre-exponential factor into a direct product of lower-dimensional ones so that $C_t(\mathbf{p}(0),\mathbf{q}(0)) \approx \prod_i^{N_{sub}} \tilde{C}_{t,i}(\tilde{\mathbf{p}}(0),\tilde{\mathbf{q}}(0))$, where N_{sub} is the number of subspaces. To understand how to better proceed, we take a two-dimensional separable system. The pre-exponential factor (4), using Eq. (13), can be written as

$$C_t(\mathbf{p}(0),\mathbf{q}(0)) = \sqrt{\det\left|\frac{1}{2}\left(\boldsymbol{M}_{\boldsymbol{qq}} + \boldsymbol{M}_{\boldsymbol{pp}} - i\hbar\boldsymbol{\Gamma}\boldsymbol{M}_{\boldsymbol{qp}} + \frac{i}{\boldsymbol{\Gamma}\hbar}\boldsymbol{M}_{\boldsymbol{pq}}\right)\right|}. \tag{15}$$

In the case of a two-dimensional separable system, the matrix components of Eq. (13) are diagonal matrices,

$$\boldsymbol{M}_{\boldsymbol{pp}} = \begin{pmatrix} M_{p_1p_1} & 0 \\ 0 & M_{p_2p_2} \end{pmatrix}, \quad \boldsymbol{M}_{\boldsymbol{pq}} = \begin{pmatrix} M_{p_1q_1} & 0 \\ 0 & M_{p_2q_2} \end{pmatrix}, \ \ldots, \text{ etc.} \tag{16}$$

Since the determinant of a block diagonal matrix is equal to the product of the block determinants, in the case of a separable system, the pre-exponential factor of Eq. (15) is given by the product of the pre-exponential factors of each dimension. This consideration suggests that the best sub-space division is the one that minimizes the off-diagonal terms of the monodromy components in Eq. (16). The elements of the monodromy matrix can be rearranged into the Jacobian matrix

$$\mathbf{J}(t) = \begin{pmatrix} \partial\mathbf{q}_t/\partial\mathbf{q}_0 & \partial\mathbf{q}_t/\partial\mathbf{p}_0 \\ \partial\mathbf{p}_t/\partial\mathbf{q}_0 & \partial\mathbf{p}_t/\partial\mathbf{p}_0 \end{pmatrix} \tag{17}$$

and, in the case of a separable system, the determinant of the full-dimensional Jacobian, $\mathbf{J}(t)$, is given by the product of the determinants of each sub-space Jacobian $\widetilde{\mathbf{J}}_i(t)$, i.e., $\det(\mathbf{J}(t)) = \prod_i^{N_{sub}} \det\left(\widetilde{\mathbf{J}}_i(t)\right)$. By virtue of Liouville's theorem, $\det(\mathbf{J}(t)) = 1$ at anytime, i.e., $d\mathbf{p}(t)\,d\mathbf{q}(t) = d\mathbf{p}(0)\,d\mathbf{q}(0)$, and, for a separable system, $\det\left(\widetilde{\mathbf{J}}_i(t)\right) = 1$ for the generic ith subspace so that $d\widetilde{\mathbf{p}}_t^i d\widetilde{\mathbf{q}}_t^i = d\widetilde{\mathbf{p}}_0^i d\widetilde{\mathbf{q}}_0^i$. However, in general, $d\widetilde{\mathbf{p}}_t d\widetilde{\mathbf{q}}_t \neq d\widetilde{\mathbf{p}}_0 d\widetilde{\mathbf{q}}_0$ and we need to look for the subspace partition which provides subspace Jacobians $\widetilde{\mathbf{J}}_i(t)$ with the closest determinants to one. Since the Jacobian is time dependent, the search for the more suitable subspace division and for the best grouping of the vibrational modes within the different subspaces also depends on time. The chosen set of M vibrational modes for a M-dimensional subspace is the one that makes the $\widetilde{\mathbf{J}}_M(t)$ determinant the closest to unity more often during the time evolution of the test trajectory, and we will refer to this procedure as the "Jacobi criterion" from now on. The selection of the best subspace dimensionality is instead performed in a hierarchical way starting from the full-dimensional space and then proceeding through the remaining degrees of freedom. More specifically, once the best M-dimensional grouping has been determined for each subspace of dimensionality $M \leq N_{vib}$, among these best subspaces of different dimensionality we choose the one for which the determinant of $\tilde{\mathbf{J}}_M(t)$ (averaged over the trajectory) is the closest to unity. Clearly, M is acceptable if it permits to achieve Monte Carlo convergence in TA-SCIVR calculations in the subspace, so it cannot be too big, otherwise the curse of dimensionality still kicks in. The same procedure is then iteratively applied for the remaining degrees of freedom until all of them have been grouped in various subspaces. The final result is a separation of the full-dimensional space into subspaces, where each subspace preserves Liouville's theorem with the best possible accuracy. The main drawback of the method is that it comes at a higher computational cost than the two previously described ones.

In Sec. III, we will apply Eqs. (11) and (7) to several systems and compare our results with the available quantum mechanical vibrational eigenvalues.

III. RESULTS AND DISCUSSION

A. A model system: Two strongly coupled Morse oscillators

To test the accuracy of Eq. (7), we consider a coupled system of the type

$$V(q_1,q_2) = D\sum_{i=1}^{2}\left[1-e^{-\alpha_i(q_i-q_i^{eq})}\right]^2 + \times c\left(q_1-q_1^{eq}\right)^2\left(q_2-q_2^{eq}\right)^2, \tag{18}$$

where the coupling is biquadratic, the dissociation energy $D = 0.2$ a.u. is the same for each oscillator, $\alpha_i = \omega_i\sqrt{\mu/2D}$, $c = 10^{-7}\mu^2$, and $q_1^{eq} = q_2^{eq} = 0$. The reduced mass μ is that of the H_2 molecule, i.e., $\mu = 918.975$ a.u., and the harmonic frequencies are 3000 and 1700 wavenumbers. The oscillators are strongly coupled as shown by the deviation of the vibrational eigenvalues from the uncoupled ones. In this case, there are two monodimensional subspaces and, as anticipated, we sample the initial phase-space conditions for the $(\tilde{\mathbf{p}}(t),\tilde{\mathbf{q}}(t))$ trajectories according to a Husimi distribution for the internal degree of freedom using a Box-Muller sampling centered at $\tilde{p}_1^{eq} = \sqrt{\omega_1}, \tilde{q}_1^{eq}$ or $\tilde{p}_2^{eq} = \sqrt{\omega_2}, \tilde{q}_2^{eq}$, with the other (external) degree of freedom initially set at equilibrium. The projection of the reference state on the subspaces is $|\tilde{\chi}\rangle = \left|\sqrt{\omega_i}, q_i^{eq}\right\rangle$, $i = \{1,2\}$. The potential of Eq. (18) provides quite a stringent test for the DC-SCIVR approach because of the artificial strong coupling. We simulate the full-dimensional and the partial-dimensional spectra both with single trajectories using the MC-SCIVR approach and with many trajectories by means of Husimi-sampled TA-SCIVR calculations. In this latter instance, we perform 10 000 trajectories 50 000 a.u. long per subspace.

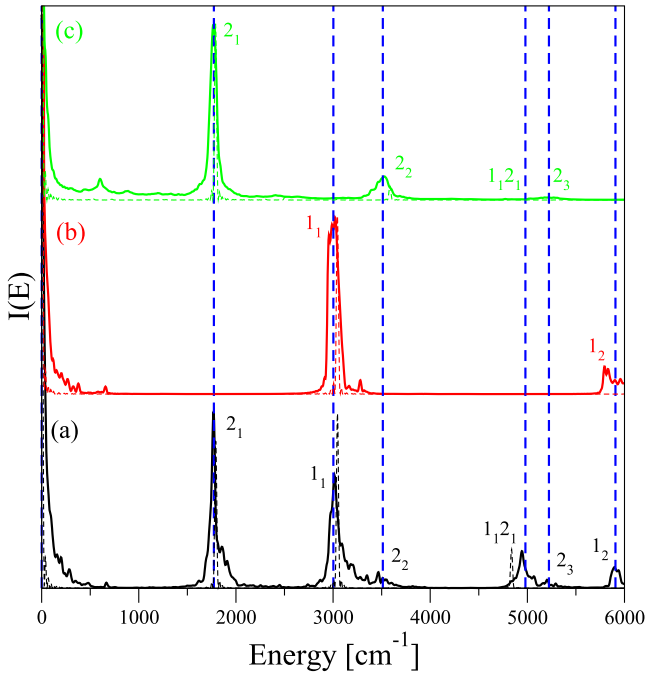

FIG. 3. DC-SCIVR spectra for the Morse oscillators of Eq. (18). Dashed lines are for the MC-SCIVR simulations and continuous ones are for 10 000-trajectory simulations. (a) The black line for the full-dimensional TA-SCIVR spectrum; (b) the red line for the DC-SCIVR spectrum of mode 1; (c) the green line, the same of (b) for mode 2. Vertical blue dashed blue lines indicate the exact values calculated by a Discrete Variable Representation (DVR) approach.[101]

The MC-SCIVR spectrum is losing accuracy only at high energies, since such energy range is not well sampled by MC-SCIVR. In the partial spectra $\tilde{I}(E)$ in Fig. 3, the overtones generated by the quantum contribution from the other subspace are much less intense and barely detectable. Nevertheless, the main spectroscopic features, i.e., fundamentals and most of the overtones, are faithfully reproduced.

B. Small molecules: H_2O, CH_2O, CH_4, and CH_2D_2

We choose H_2O, CH_2O, CH_4, and CH_2D_2 as test cases for DC-SCIVR, since these are molecular systems accessible to full-dimensional SCIVR calculations, as it has been shown in the past.[76,77,92,93] We perform full-dimensional TA-SCIVR and DC-SCIVR calculations using 30 000 a.u. long classical trajectories, which is a typical dynamics length for semiclassical calculations on molecules.[60,63,92]

For H_2O, which is the smallest of these systems, we generate 12 000 classical trajectories on the potential energy surface from Partridge and Schwenke[102] for the full-dimensional TA-SCIVR calculations, and 4000 trajectories per degree of freedom in the case of DC-SCIVR spectra. As in the case of the Morse oscillators, the reference state of each M-dimensional subspace is $|\chi\rangle = \prod_i^M \left|\sqrt{\omega_i}, q_i^{eq}\right\rangle$, where ω_i is the harmonic frequency of the i-th normal mode of vibration included in the subspace. Harmonic frequencies are listed in the "HO" column of Table I. By employing the three different subspace partition criteria previously illustrated, we find that the three vibrational degrees of freedom of water should always be grouped into two different subspaces. However, in the case of the Hessian approach, modes 1 and 2 (the bending and symmetric stretch, respectively) are separated from mode 3 (the asymmetric stretch), while the Jacobi and WSV methods suggest to collect together modes 2 and 3, leaving mode 1 alone. In Fig. 4, the DC-SCIVR spectra of water obtained with the Jacobi criterion are presented, while Table I reports the detailed computed energy levels and compares them with full-dimensional SCIVR estimates and exact values.

First of all we observe that DC-SCIVR estimates generally account pretty well for the anharmonicity of water. This can be appreciated by comparing the mean absolute deviations from quantum exact values of the DC-SCIVR estimates (~20 cm^{-1}) to the mean deviation of the harmonic frequencies (~140 cm^{-1}). In spite of the anharmonicity and intermode coupling of water, all separation criteria offer rather accurate estimates. Only in the case of the asymmetric stretch fundamental frequency the partition procedure overestimates the quantum value, which is anyway very accurately regained by the full-dimensional semiclassical approximation.

Moving to CH_2O, we sample 24 000 classical trajectories to have the full-dimensional SCIVR calculation converged on

TABLE I. Vibrational energy levels of water. The first and second columns show the vibrational state label and the exact results, respectively; the third column reports the full-dimensional TA-SCIVR eigenvalues. Column four shows the DC-SCIVR results with the Jacobi subspace criterion (DC SCIVR$_{\text{Jacobian}}$); column five refers to frequencies based on the WSV method (DC SCIVR$_{\text{WSV}}$); in column six results obtained by employing the Hessian matrix criterion (DC SCIVR$_{\text{Hess}}$) are listed. The last column reports the harmonic estimates HO. All values are in cm^{-1}. MAE stands for mean absolute error and it is calculated with respect to the exact values[102] and for DC-SCIVR simulations also with respect to the full-dimensional TA-SCIVR values. Values for DC SCIVR$_{\text{Jacobi}}$ and DC SCIVR$_{\text{WSV}}$ are exactly the same because they are based on exactly the same partition of the vibrational modes into the two work subspaces.

Mode	Exact[102]	TA SCIVR	DC SCIVR$_{\text{Jacobi}}$	DC SCIVR$_{\text{WSV}}$	DC SCIVR$_{\text{Hess}}$	HO
1_1	1595	1580	1584	1584	1581	1649
1_2	3152	3136	3164	3164	3154	3298
2_1	3657	3664	3668	3668	3656	3833
3_1	3756	3760	3802	3802	3824	3944
MAE exact		11	20	20	21	141
MAE SCIVR			20	20	23	

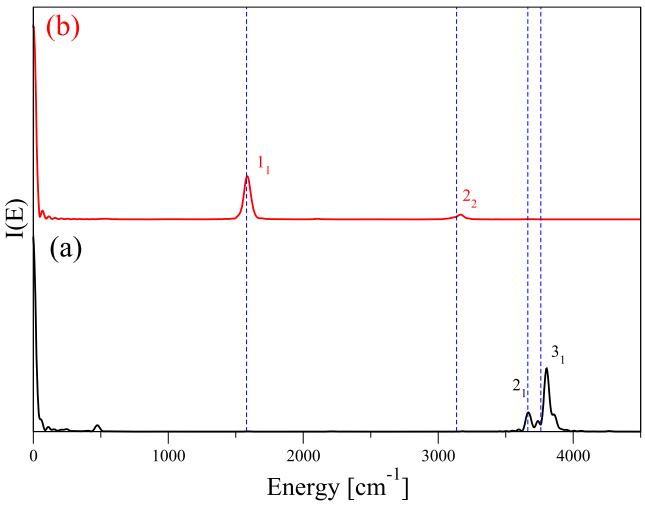

FIG. 4. DC-SCIVR vibrational spectra of H_2O. The black line in panel (a) reports the two-dimensional subspace spectrum and the red line in panel (b) reports the monodimensional one. Vertical blue dashed lines are the full-dimensional TA-SCIVR values.

the potential energy surface constructed by Martin *et al.*[103] To keep the same overall computational cost, we take 4000 trajectories per degree of freedom when calculating the partial spectra. The dimensionality of each subspace for the DC-SCIVR calculations is chosen by employing the three criteria introduced in Sec. II. In the case of the Hessian matrix criterion, we find that for a value of $\epsilon = 3.0 \cdot 10^{-7}$, the full six-dimensional vibrational space is partitioned into a three-dimensional, a bi-dimensional, and a mono-dimensional subspace. When using the WSV approach, the biggest subspace dimensionality is four for a threshold value of $\epsilon_B = 120$. When employing the Jacobi criterion, the division turns out to be different. Figure 5 shows the displacement of the determinant of the reduced-dimensional Jacobian matrix, i.e., $\det\left(\tilde{\mathbf{J}}_i(t)\right)$ calculated on the basis of the projected trajectories $\tilde{\mathbf{p}}(t), \tilde{\mathbf{q}}(t)$, from unity for different choices of the subspace dimensionality M in the case of CH_2O, CH_4, and CH_2D_2. Clearly, there is no approximation for the full-dimensional analyses. For the CH_2O molecule, the smallest deviation is obtained for a maximum subspace dimensionality equal to 4, which

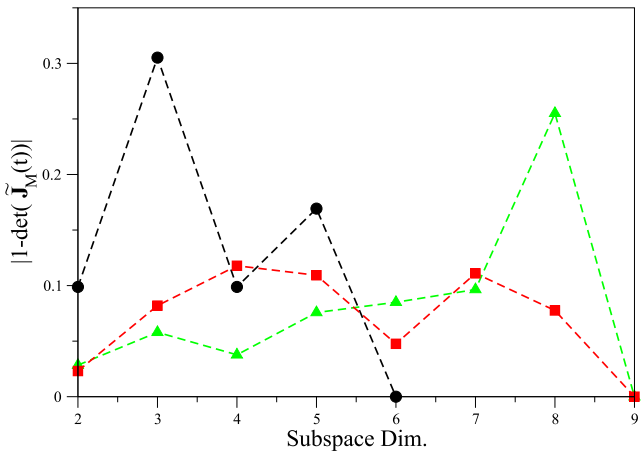

FIG. 5. Average values of $\left|1 - \det\left(\tilde{\mathbf{J}}_M(t)\right)\right|$ for the best grouping for different subspace dimensionalities M. Black filled circles for CH_2O, red filled squares for CH_4, and green filled triangles for CH_2D_2.

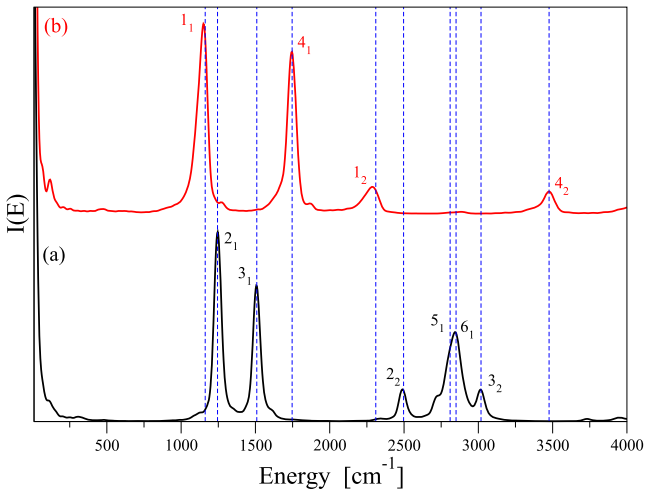

FIG. 6. DC-SCIVR vibrational spectra of CH_2O. The black line in panel (a) reports the four-dimensional subspace spectrum and the red line in panel (b) reports the bi-dimensional one. Vertical blue dashed lines are the full-dimensional TA-SCIVR values.

is slightly better than a bi-dimensional choice. After setting these four normal modes into the same subspace, the other two left modes are taken in the same subspace. Eventually the initial full-dimensional space is divided into 4- and 2-dimensional ones. The corresponding spectra are reported in Fig. 6. As a comparison, the full-dimensional TA-SCIVR values are reported as vertical blue dashed lines. All vibrational features are faithfully reproduced, including overtones. It may be noticed that the signals of the fifth and sixth fundamentals sum up to a broader peak in the 4-dimensional spectrum. They can be separated by inserting the parity symmetry into the reference state when performing the 4-dimensional simulation. This common practice in semiclassical calculations permits us to enhance the signal of one vibration at a time.[58,77] To have a more detailed comparison, Table II shows DC-SCIVR results, the exact ones,[104] and the full-dimensional SCIVR frequencies.

To help the reader to better appreciate the level of accuracy for each semiclassical approximation, we report in the last lines the Mean Absolute Error (MAE). The DC-SCIVR deviation with respect to the exact value is 12 cm^{-1} for the Jacobi and WSV approaches and 25 cm^{-1} for the Hessian one. These values are comparable with the full-dimensional TA-SCIVR one of 9 cm^{-1}. Conversely, a harmonic estimate is almost three times less accurate than the DC-SCIVR ones. When comparing the approximate DC-SCIVR results with the TA-SCIVR ones, the deviation is on average really small, respectively, 6 cm^{-1}, 6 cm^{-1}, and 19 cm^{-1} for the Jacobi, WSV, and Hessian criteria.

In the case of the CH_4 molecule, we employ the potential energy surface (PES) by Lee *et al.*[105] Given the highly chaotic regime for the classical trajectories of this PES, about 95% of the trajectories have been rejected due to the deviation of the full-dimensional monodromy matrix determinant from unity. By employing an amount of 180 000 trajectories, we still have enough trajectories left for TA-SCIVR Monte Carlo convergence. When dividing the space into subspaces, we keep the number of trajectories per degree of freedom equal to 20 000, in order to have for the overall DC-SCIVR calculation the

TABLE II. The same as in Table I this time for the vibrational energy levels of CH_2O.

Mode	Exact[104]	TA SCIVR	DC SCIVR$_{Jacobi}$	DC SCIVR$_{WSV}$	DC SCIVR$_{Hess}$	HO
1_1	1171	1162	1154	1154	1192	1192
2_1	1253	1245	1246	1246	1244	1275
3_1	1509	1509	1508	1508	1508	1544
4_1	1750	1747	1746	1746	1755	1780
1_2	2333	2310	2288	2288	2286	2384
2_2	2502	2497	2490	2490	2423	2550
5_1	2783	2810	2816	2816	2836	2930
6_1	2842	2850	2845	2845	2864	2996
3_2	3016	3018	3016	3016	3024	3088
4_2	3480	3476	3478	3478	3486	3560
MAE exact		9	12	12	25	66
MAE SCIVR			6	6	19	

same total amount of trajectories. We have recently shown[75] that when a value of $\epsilon = 4.8{\cdot}10^{-7}$ is employed for the Hessian criterion, the nine-dimensional vibrational space of methane is decomposed into six-dimensional and three-dimensional ones. When applying the WSV criterion with $\epsilon_B = 85$, we also obtain a six-dimensional and a three-dimensional subspace. Finally, even on the basis of the Jacobi criterion, the better choice for the maximum dimensional subspace is six, as shown in Fig. 5. We then hierarchically apply the same criterion for the remaining vibrational modes and find out that a division into a bi-dimensional plus a mono-dimensional subspace is preferred with respect to a single three-dimensional one. Eventually, the nine-dimensional vibrational space is partitioned into six-, two-, and mono-dimensional ones. Figure 7 reports the partial spectra of the three subspaces. Given the degeneracy of some of methane vibrations, the nine vibrational modes are labeled in four groups. Since degenerate modes can be projected onto different subspaces, spectral contributions to the same peak may be observed in Fig. 7 from different spectra. The full-dimensional TA-SCIVR peaks are once again well reproduced, including overtones and combination of overtones. Vibrations 4_1 and 2_2 have been separated by including the parity symmetry into the reference state. For a detailed comparison, we report in Table III our vibrational eigenvalues and compare them with the exact ones. On average, the full-dimensional TA-SCIVR is quite accurate, i.e., there is only a 12 cm^{-1} difference from the exact frequency. The DC-SCIVR accuracy using the Jacobi criterion is slightly worse (MAE = 17 cm^{-1}), and it is comparable when using either the WSV or the Hessian criterion. These deviations are about six times more accurate than a crude harmonic approximation. Finally, a comparison among the different semiclassical approaches shows that in this case the Hessian criterion provides slightly more accurate results than the Jacobi ones. However, it is the overtone excitation 1_2 which is responsible for the slightly worse accuracy of the Jacobi criterion with respect to the Hessian one. If one did not consider this term on the MAE calculation, the Jacobi DC-SCIVR estimate would be on average within 9 cm^{-1} of the exact one and only 6 cm^{-1} away from the TA-SCIVR value.

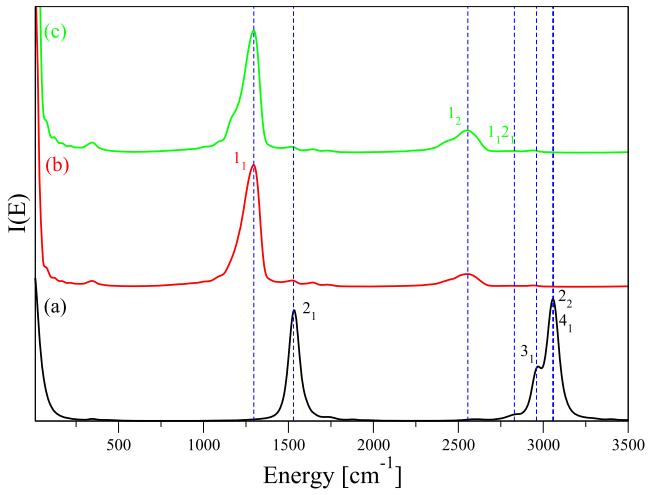

FIG. 7. DC-SCIVR vibrational spectra of methane. Black line in panel (a) reports the six-dimensional subspace partial spectrum, the red line in panel (b) reports the bi-dimensional one, and the green line in panel (c) reports the mono-dimensional one. Vertical blue dashed lines indicate the full-dimensional TA-SCIVR values.

Finally, we look at the lower symmetry molecule CH_2D_2, where some of the typical degenerations of methane have been removed. We employ the same PES as in the case of CH_4 and experience a comparable percentage of trajectory rejection for the monodromy matrix evolution in a chaotic potential. As above, we choose to employ 180 000 trajectories. Using the Hessian matrix criterion at a value $\epsilon = 2{\cdot}10^{-7}$, we obtain a decomposition of the full nine-dimensional space into a six-dimensional and a three-dimensional one. According to the WSV criterion, at a value $\epsilon_B = 180$, we obtain a decomposition of the full nine-dimensional space into a four-dimensional, a three-dimensional, and a bi-dimensional one. In the Jacobi approach reported in Fig. 5, we look at the green triangle profile and conclude that a four-dimensional subspace is the first step in the hierarchical determination of the subspaces. Then, among the remaining five-dimensional modes, the Jacobi analysis leads to a partition into a three- and a two-dimensional subspace. Eventually, the nine-dimensional space is divided into four-, three-, and two-dimensional subspaces.

TABLE III. The same as in Table I but for the vibrational energy levels of CH_4.

Mode	Exact[106]	TA SCIVR	DC SCIVR$_{Jacobi}$	DC SCIVR$_{WSV}$	DC SCIVR$_{Hess}$[75]	HO
1_1	1313	1300	1296	1308	1300	1345
2_1	1535	1529	1530	1530	1532	1570
1_2	2624	2594	2556	2588	2606	2690
$1_1 2_1$	2836	2825	2830	2832	2834	2915
3_1	2949	2948	2960	2933	2964	3036
2_2	3067	3048	3060	3044	3050	3140
4_1	3053	3048	3056	3038	3044	3157
MAE exact		12	17	15	11	68
MAE SCIVR			11	7	7	

Figure 8 reports the partial spectra for the four-dimensional (a), the three-dimensional (b), and the two-dimensional (c) subspaces. By comparison with the dashed vertical lines representing the full-dimensional semiclassical results, we can observe that some accuracy is lost for the combined overtones (see the $1_1 2_1$ peak) with respect to the typical accuracy of the fundamental peaks, as it was noticed for the strongly coupled Morse oscillators.

Table IV shows the computed DC-SCIVR energy levels which are compared with both the exact values[106] and the full-dimensional TA-SCIVR ones. For this system, the MAEs relative to the exact values are more accurate for the TA-SCIVR and the Jacobian DC-SCIVR than for the standard Hessian criterion. When comparing the different semiclassical approaches the expected order is found, i.e., from the more accurate TA-SCIVR to the less accurate DC-SCIVR.

C. A complex and strongly anharmonic molecular system: $H_5O_2^+$

We keep proceeding in the application of DC-SCIVR to larger and larger molecules and face the challenge represented by the Zundel cation. $H_5O_2^+$ with its 15 vibrational degrees of freedom has attracted the interest of many, mainly due to the vibrational features related to the motion of the shared proton. Specifically, a doublet is found in the vibrational predissociation spectra of Zundel ions in the region of the O–H–O stretch associated with the proton transfer (~1000 cm^{-1}). Furthermore, two neatly separated bending signals are present owing to the water bending-proton transfer interaction.[107,108] Consequently in our investigation we focus our attention on the proton transfer doublet, the water bendings, and, in addition, the four high-frequency free OH stretchings which are well detected by experimental spectra.[109] We benchmark our DC-SCIVR simulations against the Multi Configuration Time Dependent Hartree (MCTDH) calculations of Meyer *et al.*[107,110–115] and also compare them with the Vibrational Configuration Interaction (VCI) estimates of Bowman and collaborators.[116]

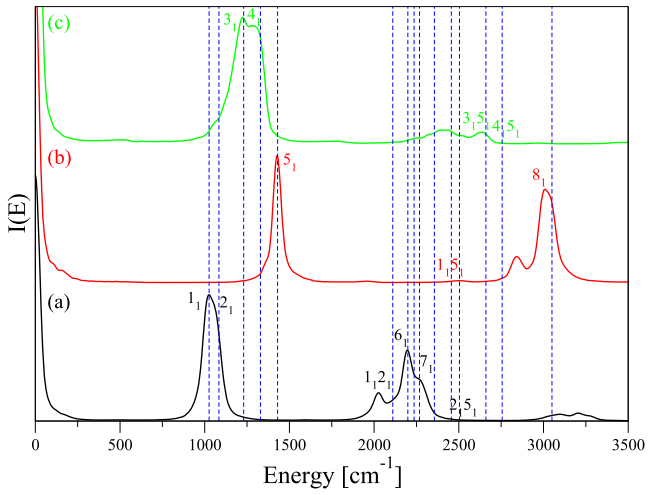

FIG. 8. DC-SCIVR vibrational spectra of the CH_2D_2 molecule. The black line in panel (a) reports the partial spectrum for the 4-dimensional subspace, the red line in panel (b) reports the three-dimensional one, and the green line in panel (c) reports the bi-dimensional one. Vertical blue dashed lines are the full-dimensional TA-SCIVR values.

We propagate the test classical trajectory on an accurate $H_5O_2^+$ PES.[117] The trajectory is characterized by a strongly roto-vibrationally coupled motion leading to monodromy matrix instability and to a couple of hindrances to the application of our semiclassical techniques. For this reason, a Jacobi-based subspace partition is not feasible and we have to rely on the Hessian method to determine our work subspaces. Also, the coupling is responsible for an exaggerated broadening of the spectral features. This latter drawback can be overcome by removing the Cartesian angular momentum every few steps along the dynamics of the trajectories employed in our calculations. The associated loss in energy may partially affect the frequency accuracy (an artificial shift towards their harmonic counterparts is anticipated for the high frequencies) but it is compensated by the Husimi distribution of energies around the harmonic zero-point one employed for the initial conditions. Finally, due to the monodromy matrix instability, the original Herman-Kluk prefactor cannot be employed, so we approximate it by means of a reliable second-order iterative approximation that depends only on the Hessian matrix.[93] As expected, peaks in the spectra still not only have good accuracy but they are also much narrower thus decreasing the uncertainty of our results.

The Hessian criterion suggests us to enroll the normal modes associated with the free OH stretchings of the two water molecules into a four-dimensional subspace, while all the other degrees of freedom are grouped into mono-dimensional subspaces. For this reason, we assign the two water bendings to two separate mono-dimensional subspaces, and the same fate

TABLE IV. The same as in Table I but for the vibrational energy levels of CH_2D_2.

Mode	Exact[106]	TA SCIVR	DC SCIVR$_{Jacobi}$	DC SCIVR$_{WSV}$	DC SCIVR$_{Hess}$	HO
1_1	1034	1026	1028	1020	1038	1053
2_1	1093	1084	1072	1098	1086	1116
3_1	1238	1230	1234	1212	1230	1266
4_1	1332	1329	1320	1326	1316	1360
5_1	1436	1430	1430	1420	1434	1471
1_12_1	2128	2110	2089	2080	2114	2169
6_1	2211	2199	2195	2192	2137	2236
1_13_1	2242	2236	2250	2231	2210	2319
7_1	2294	2268	2274	2250	2274	2336
1_14_1	2368	2356	/	/	2400	2413
1_15_1	2474	2456	2485	2436	2484	2524
2_15_1	2519	2504	2516	2494	2510	2587
3_15_1	2674	2660	2661	2672	2627	2737
4_15_1	2769	2756	2754	2734	/	2831
8_1	3008	3050	3000	3012	3026	3103
MAE exact		14	13	21	21	47
MAE SCIVR			12	15	19	

applies to the mode associated with the shared proton motion. The only exception concerns the O–O stretching mode which is collected with a wagging state into a bi-dimensional subspace. This choice is driven by previous studies that have provided evidence of the occurrence of a combined state interacting with the shared proton motion.[107,111] We run 2000 full-dimensional classical trajectories per degree of freedom, i.e., 2000 for the mono-dimensional subspaces, 4000 for the bi-dimensional one, and 8000 for the four-dimensional subspace. For each subspace, the initial kinetic energy is given in the usual harmonic fashion to the four OH stretches and to the modes enrolled in the subspace under investigation. No energy is instead given to the other modes.

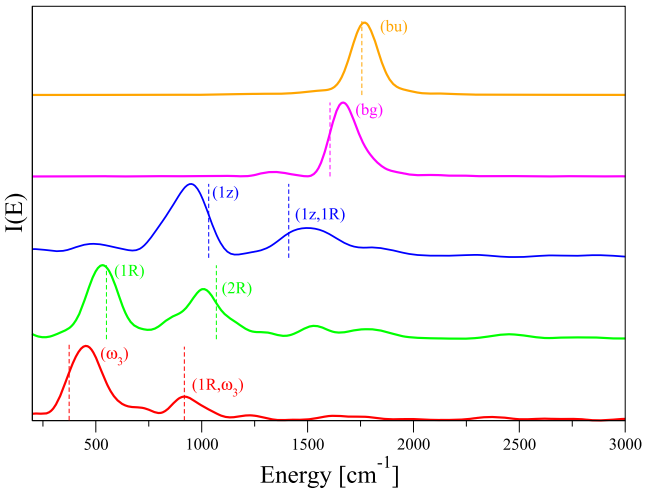

FIG. 9. Vibrational spectra of the Zundel cation. Starting from the top, orange, magenta, and blue lines report the spectra of the mono-dimensional subspaces associated with the (*bu*), (*bg*), and (1*z*) excitations; the green and red lines build up together the bi-dimensional subspace. The zero point energy value has been shifted to the origin in each subspace to help the reader in comparing the different frequencies. The vertical dashed lines indicate the MCTDH reference.[107]

Figure 9 reports the main excitations below 2000 wavenumbers. To remove any spurious noise effect, we add a Gaussian filter of type $e^{-\alpha t^2}$ in the Fourier transform, with $\alpha = 3{\cdot}10^{-8}$ a.u. The orange and magenta lines refer to the two water bendings (*bu*) and (*bg*); the blue line shows the signal of the shared proton motion (1*z*) and a mixed excitation (1*z*, 1*R*). Finally, on the bottom of the figure are the spectra associated with the bi-dimensional subspace. The usual procedure based on selecting the parity of the semiclassical reference state permits us to separate the overlapping features of this bidimensional subspace. Specifically, in green the fundamental for the O–O stretch (1*R*) and its overtone (2*R*) are detected, while in red the excitation ω_3 of the wagging state (assigned on the basis of the MCTDH benchmark) and the combined excitation $(1R, \omega_3)$ stand out. In Fig. 10 are instead illustrated

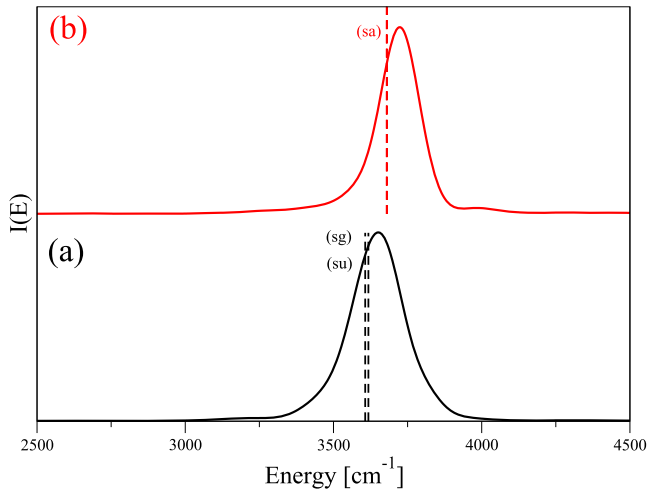

FIG. 10. Vibrational spectra of the Zundel cation in the free OH stretching region. Starting from the bottom, panel (a) reports the spectrum of (*sg*) and (*su*), and panel (b) refers to (*sa*) excitations. The zero point energy value has been shifted to the origin to help the reader in evaluating the frequencies of the peaks. The vertical dashed lines indicate the MCTDH estimates.[107]

TABLE V. Vibrational energy levels of the Zundel cation reported in cm^{-1}. The first column presents the label of the excitation according to Ref. 107. The second column contains the experimental values, the third and fourth ones show the MCTDH results from two different studies,[107,111] while in the fifth column, our DC-SCIVR estimates are reported. Column six contains the VCI energy levels[116] and, finally, in the last column are the harmonic estimates of the fundamental excitations. The last row reports the mean absolute error of the DC-SCIVR estimates with respect to the benchmark MCTDH values of Ref. 107.

Label	Expt.[109]	MCTDH[107]	MCTDH[111]	DC SCIVR	VCI[116]	HO
(ω_3)[a]		374	386	452		
(1R)		550		532		630
$(1R, \omega_3)$	928	918	913	920		
(1z)	1047	1033	1050	952	1070	861
(2R)		1069		1008		
$(1z, 1R)$	1470	1411	1392	1520	1600	
bg		1606		1668	1604	1720
bu	1763	1756	1756	1768	1781	1770
sg		3607		3650	3610	3744
su	3603	3614	3618	3650	3625	3750
sa	3683	3689	3680	3720	3698	3832
MAE				46		

[a]This assignment of the ω_3 wagging excitation is done upon comparison to the benchmark MCTDH values.

the DC-SCIVR spectra of the free OH stretchings. In panel (a) the spectra of the (*sg*) and (*su*) excitations are reported, while panel (b) shows the signal of the two remaining OH stretchings labeled as (*sa*).

Table V shows our computed energy levels, labeled with the usual nomenclature for the Zundel cation reported in the literature.[107,111] Our DC-SCIVR estimates are pretty accurate with the exception of the combined excitation $(1z, 1R)$ which is rather off-the-mark, but anyway better than the VCI value. A certain degree of inaccuracy arises also for the (1z) signal. As anticipated, the high frequency estimates are blue shifted with respect to the benchmark values, an effect the instantaneous removal of the Cartesian angular momentum may have largely contributed to. Overall, the average deviation from MCTDH results is 46 wavenumbers that decreases to 38 if $(1z, 1R)$ is not considered. These values are not far from those found for smaller molecules and are satisfactory given the high complexity of the Zundel cation.

D. "Divide-and-conquer" semiclassical dynamics for a high dimensional molecule: Vibrational power spectrum of benzene

Halverson and Poirier have recently calculated the vibrational frequencies of benzene using a discrete variable representation (DVR) approach. They pushed the limits of "exact" vibrational state calculations up to thirty dimensions.[78] In their method, the DVR basis set and grid has been conveniently selected using phase-space localized basis (PSLB) sets and truncated Harmonic Oscillator Basis (HOB) functions.[3,4,118] They were able to obtain all the relevant (about a million) vibrational energy levels of benzene within a given energy threshold. They employed a quartic force field modeling for the PES.[119]

We employ the same surface for a direct comparison between the present DC-SCIVR method and the exact DVR one. First we study how to best partition the 30-dimensional space. Using the Hessian-based approach and $\epsilon = 9{\cdot}10^{-7}$, the full-dimensional space is separated into one eight-dimensional subspace, eight bi-dimensional subspaces, and six mono-dimensional subspaces. When employing the WSV criterion and $\epsilon_B = 5.6{\cdot}10^3$, the full-dimensional space is partitioned into one ten-dimensional subspace, two seven-dimensional subspaces, and one six-dimensional subspace. When using the Jacobian-based criterion, the computational search for space decomposition is much more computationally expensive since all possible combinations of the 30 vibrational modes into groups of M should be tested. We restrict instead our search to $6 \leq M \leq 10$ since the Hessian criterion shows that when the biggest subspace is eight-dimensional then the results are quite accurate. We cannot rule out that there may be a better choice for $M > 10$. However, the potential little improvement in the accuracy of the results does not justify the additional huge computational overhead.

Figure 11 shows the result of this search and points to a seven-dimensional subspace for the first partition. The same procedure is repeated and involves the remaining 23 modes.

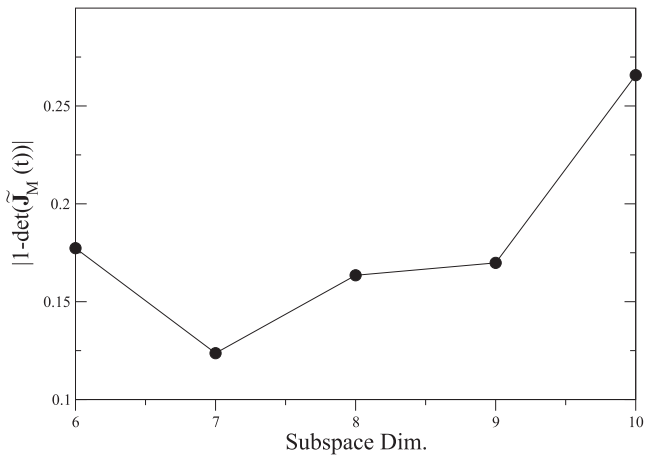

FIG. 11. Values of $\left|1 - \det\left(\tilde{\mathbf{J}}_M(t)\right)\right|$ for different choices of the subspace dimensionality M for the C_6H_6 molecule.

TABLE VI. Benzene DC-SCIVR vibrational frequencies compared with available quantum results (EQD). Degenerate frequencies are not replicated. Values are given in cm^{-1}.

State	HO	DC $SCIVR_{WSV}$	DC $SCIVR_{Jacobi}$	EQD	State	HO	DC $SCIVR_{WSV}$	DC $SCIVR_{Jacobi}$	EQD
1_1	407	432	399	399.4554	11_1	1167	1150	1144	1147.751
2_1	613	610	606	611.4227	12_1	1192	1189	1175	1180.374
3_1	686	610	696	666.9294	2_2	1226	1223	1228	1221.27
4_1	718	742	719	710.7318	13_1	1295	1330	1314	1315.612
5_1	866	865	869	868.9106	14_1	1390	1375	1352	1352.563
6_1	989	990	997	964.0127	4_2	1436	1410	1437	1418.58
7_1	1011	1038	1020	985.8294	15_1	1512	1464	1492	1496.231
8_1	1008	1002	990	997.6235	16_1	1639	1614	1602	1614.455
9_1	1024	1014	1014	1015.64	5_2	1732	/	1752	1737.51
10_1	1058	1042	1042	1040.98	MAE		15	9	

The second subspace found is a six-dimensional one. The third search (among the remaining 17 modes) leads to a ten-dimensional subspace. The remaining seven modes are collected together within the same subspace. Eventually, the full thirty-dimensional vibrational space has been partitioned into a ten-dimensional subspace, two seven-dimensional subspaces, and one six-dimensional subspace. Whatever the method employed for partitioning the space, we run 1000 trajectories per degree of freedom to calculate the frequencies. Each trajectory is 30 000 a.u. long. To remove any spurious noise effect, in the Fourier transform, we add the same Gaussian filter used for the Zundel cation. As usual, the reference state of each M-dimensional subspace is written as $|\chi\rangle = \prod_i^M \left|\sqrt{\omega_i}, q_i^{eq}\right\rangle$, where ω_i are the harmonic frequencies that we report under the columns "HO" in Table VI. For the evolution of the pre-exponential factor (4) and its phase calculation, we use a recently introduced iterative second-order approximation.[93] This approximation allows for the calculation of the pre-exponential factor without explicitly calculating the monodromy matrix elements, and it can be safely employed for strongly chaotic and high-dimensional systems, as in the case of the benzene molecule. Figure 12 shows our computed spectra. Panel (a) reports the six-dimensional subspace, panels (b) and (c) report the seven-dimensional ones, and panel (d) reports the 10-dimensional subspace.

We follow Halverson and Poirier in their labeling of vibrational states. Table VI reports our computed energy levels compared with the available exact ones. We find an excellent agreement with a MAE of only 9 wavenumbers when adopting Jacobi's criterion. With the WSV approach, the MAE increases to 15 cm^{-1}. As we have recently reported,[75] the Hessian criterion leads to still acceptable but less accurate results, with a MAE of 19 wavenumbers.

Despite the increase in dimensionality, we conclude that moving from the four smaller molecular systems of Sec. III B to benzene, the MAE referred to the exact results is anyway limited to 10-20 cm^{-1}, a proof of the reliability of DC-SCIVR and of the accuracy of the new Jacobian criterion.

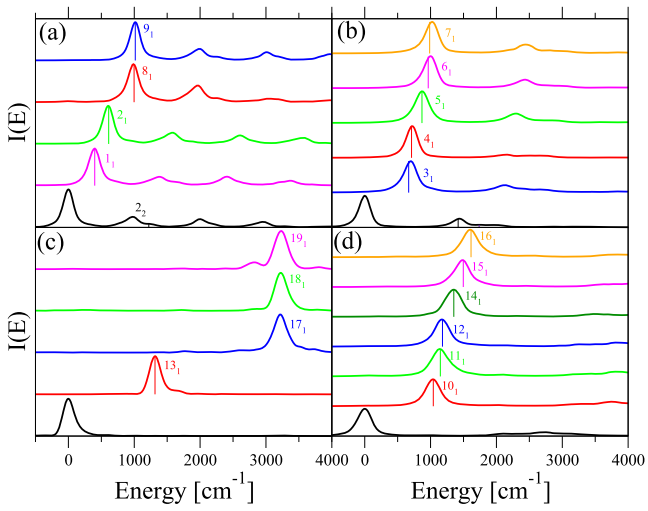

FIG. 12. Vibrational spectra of C_6H_6 as obtained upon partition of the full-dimensional space according to the Jacobian criterion. Panel (a) reports the features of the six-dimensional subspace. Panels (b) and (c) contain the spectra of the two seven-dimensional subspaces, while panel (d) refers to the 10-dimensional subspace. The zero point energy value has been shifted to the origin to help the reader in evaluating the frequencies of the other peaks. The vertical lines indicate the exact levels from Poirier's EQD calculations.[78]

IV. SUMMARY AND CONCLUSIONS

All quantum mechanical methods suffer from the curse of dimensionality. In this paper, we have illustrated a method to deal with it and to obtain vibrational frequencies almost as accurate as in standard SCIVR simulations, i.e., just a few wavenumbers away from the exact quantum values. More specifically, a "*divide et impera*" strategy has been adopted, in which spectra are calculated in partial dimensionality even if they are still based on full-dimensional classical trajectories. The method does not take advantage in any way of molecular symmetry.

We have shown how crucial the choice of the criterium for the decomposition of the full-dimensional space into mutually disjoint subspaces can be. In particular, the partition procedure based on the Jacobian matrix is the one that usually minimizes the error in approximating the full-dimensional pre-exponential factor as the direct product of several reduced dimensionality ones. This is evident from Fig. 13 where DC-$SCIVR_{Jacobi}$ is clearly the overall more accurate way to decompose the vibrational space. The exception of CH_4 is due to a not very accurate estimate of a single overtone which we have anyway included in the MAE calculation, while the Jacobian-based partition strategy remains the most accurate

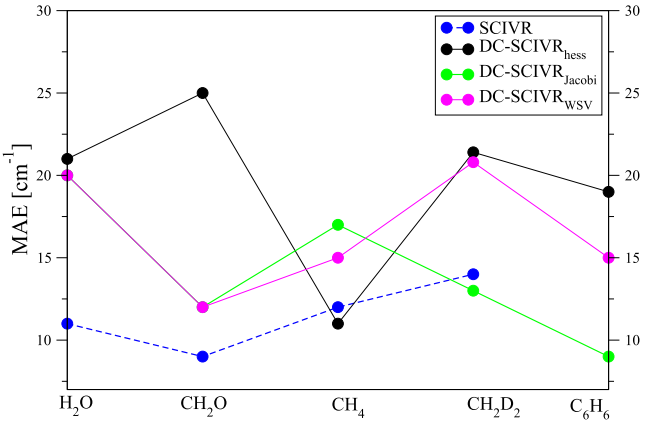

FIG. 13. Trend of the mean absolute error (MAE) with respect to exact results for the different molecules investigated. Results refer to full-dimensional SCIVR calculations (blue), DC-SCIVR with Hessian matrix criterion (black), DC-SCIVR with Jacobian matrix criterion (green), and DC-SCIVR with WSV subspace partition (magenta).

even for CH_4 as far as fundamental frequencies are concerned. The apparent better accuracy of DC-SCIVR$_{Jacobi}$ with respect to the full-dimensional calculation for CH_2D_2 is to be ascribed instead to an accidental compensation of errors between the semiclassical and subspace-partition approximations. Another key advantage of the Jacobian-based approach lies on its less noisy spectra with better resolved peaks, which is going to be more and more evident and helpful as the dimensionality of the system increases. Remarkably, the Jacobi criterion provides an internally consistent method to check the reliability of the subspace partition. In fact, not always an increase in the subspace dimensionality leads to more accurate vibrational frequencies. On the contrary, spectra can be noisier or it could be even impossible to collect a sensible spectral signal. The partitioning schemes here developed can be also adopted for on-the-fly DC-SCIVR calculations. In fact, upon calculation of the test trajectory and of the associated Hessians and monodromy matrix elements by means of *ab initio* molecular dynamics, it is possible to determine the best subspace partition by following exactly the same procedures and at no additional cost with respect to DC-SCIVR simulations based on analytical potential energy surfaces.

DC-SCIVR, like other semiclassical and classical methods, is based on the Fourier transform of a survival amplitude. According to Nyquist's theorem, for a total evolution time T, a peak width equal to $2\pi/T$ should be expected. In our simulations, though, other factors contribute to increase the width of the spectral features. The ro-vibrational coupling generates a vibrational angular momentum which perturbs the pure vibrational motion. Furthermore, when a Gaussian filter is employed, peaks may be substantially enlarged (as in the case of $H_5O_2^+$ and benzene). The full width at half maximum (FWHM) of the peaks provides a measure of the uncertainty of our results and benchmark values are always within this uncertainty bar. A potential drawback related to the width of the peaks is that it may hinder the resolution of spectral features very close to each other. A practical way to overcome this issue, which is largely adopted in semiclassical dynamics, consists in employing a proper combination of coherent states able to introduce a parity symmetry[77,92] which permits to distinguish among spectral features belonging to different vibrational modes.

A known issue of semiclassical spectra is represented by the so-called "ghost" peaks. These are unphysical features that can be generally distinguished from the true fundamental transitions because of their much lower intensity. As shown in Fig. 3, this is not a specific drawback of DC-SCIVR simulations since full-dimensional calculations present the same issue. The adoption of a combination of coherent states able to account for the parity symmetry further enhances this discrepancy in the intensities making the identification of the true vibrational features even more favored.

DC-SCIVR can be employed to simulate all kinds of spectroscopies relative to the nuclear motion, such as IR, Raman, absorption/emission dipole, vibro-electronic, and photodetachment spectra. It will allow us to read each part of the spectra in a wider molecular context up to the nanoscale, with inclusion of non-trivial long-range quantum interactions. The calculation of partial spectra representations has not only the advantage to accelerate the Monte Carlo integration by virtue of the reduced dimensionality of each subspace and to get better resolved spectra but also simplifies the identification of each peak. Another potential application of DC-SCIVR is in the field of mixed (hybrid) semiclassical methods[87,120,121] due to the possibility to assign different degrees of freedom to the different semiclassical techniques employed.

In conclusion, we think that semiclassical molecular dynamics is a very convenient approach for quantum mechanical simulations of nuclear vibrational spectroscopy. Future challenges, concerning the study of vibrational features of large molecules involved in biological mechanisms and technological processes, will be tackled in a novel quantum-mechanical fashion thanks to DC-SCIVR and the implementation of the newly proposed subspace-separation criterion.

ACKNOWLEDGMENTS

Professor Bill Poirier is gratefully acknowledged for providing the potential energy surface of benzene and the results of his quantum simulations. Professors Jiri Vaníček and Frank Grossmann and Dr. Max Buchholz are warmly thanked for their comments on a preliminary draft of the paper, and an anonymous referee is thanked for suggesting the water and Zundel cation applications. We acknowledge financial support from the European Research Council (ERC) under the European Union's Horizon 2020 research and innovation programme (Grant Agreement No. [647107]–SEMICOMPLEX–ERC-2014-CoG). We thank Università degli Studi di Milano for further computational time at CINECA (Italian Supercomputing Center) and the Regione Lombardia award under the LISA initiative (grant GREENTI) for the availability of high performance computing resources.

[1]J. M. Bowman, T. Carrington, and H.-D. Meyer, Mol. Phys. **106**, 2145 (2008).
[2]G. Avila and T. Carrington, Jr., J. Chem. Phys. **135**, 064101 (2011).
[3]G. Avila and T. Carrington, Jr., J. Chem. Phys. **134**, 054126 (2011).
[4]G. Avila and T. Carrington, Jr., J. Chem. Phys. **137**, 174108 (2012).
[5]P. S. Thomas and T. Carrington, Jr., J. Phys. Chem. A **119**, 13074 (2015).
[6]V. Barone, J. Chem. Phys. **122**, 014108 (2005).

[7]C. Puzzarini, M. Biczysko, and V. Barone, J. Chem. Theory Comput. **6**, 828 (2010).
[8]C. Puzzarini, M. Biczysko, and V. Barone, J. Chem. Theory Comput. **7**, 3702 (2011).
[9]M. Biczysko, J. Bloino, I. Carnimeo, P. Panek, and V. Barone, J. Mol. Struct. **1009**, 74 (2012).
[10]O. Bludsky, J. Chocholousova, J. Vacek, F. Huisken, and P. Hobza, J. Chem. Phys. **113**, 4629 (2000).
[11]J. Bloino, A. Baiardi, and M. Biczysko, Int. J. Quantum Chem. **116**, 1543 (2016).
[12]M. K. Petersen, F. Wang, N. P. Blake, H. Metiu, and G. A. Voth, J. Phys. Chem. B **109**, 3727 (2005).
[13]K. Vanommeslaeghe, E. Hatcher, C. Acharya, S. Kundu, S. Zhong, J. Shim, E. Darian, O. Guvench, P. Lopes, I. Vorobyov *et al.*, J. Comput. Chem. **31**, 671 (2010).
[14]J. Wang, R. M. Wolf, J. W. Caldwell, P. A. Kollman, and D. A. Case, J. Comput. Chem. **25**, 1157 (2004).
[15]G. Mathias, S. D. Ivanov, A. Witt, M. D. Baer, and D. Marx, J. Chem. Theory Comput. **8**, 224 (2011).
[16]M.-P. Gaigeot, Phys. Chem. Chem. Phys. **12**, 3336 (2010).
[17]M. Thomas, M. Brehm, R. Fligg, P. Vöhringer, and B. Kirchner, Phys. Chem. Chem. Phys. **15**, 6608 (2013).
[18]J. Gomez Llorente and E. Pollak, Annu. Rev. Phys. Chem. **43**, 91 (1992).
[19]R. Iftimie, P. Minary, and M. E. Tuckerman, Proc. Natl. Acad. Sci. U. S. A. **102**, 6654 (2005).
[20]S. Pratihar, X. Ma, Z. Homayoon, G. L. Barnes, and W. L. Hase, J. Am. Chem. Soc. **139**, 3570 (2017).
[21]H. B. Schlegel, J. M. Millam, S. S. Iyengar, G. A. Voth, A. D. Daniels, G. E. Scuseria, and M. J. Frisch, J. Chem. Phys. **114**, 9758 (2001).
[22]E. J. Heller, Acc. Chem. Res. **14**, 368 (1981).
[23]M. F. Herman and E. Kluk, Chem. Phys. **91**, 27 (1984).
[24]S. V. Antipov, Z. Ye, and N. Ananth, J. Chem. Phys. **142**, 184102 (2015).
[25]A. R. Walton and D. E. Manolopoulos, Chem. Phys. Lett. **244**, 448 (1995).
[26]Y. Elran and K. Kay, J. Chem. Phys. **110**, 3653 (1999).
[27]K. G. Kay, J. Chem. Phys. **101**, 2250 (1994).
[28]K. G. Kay, J. Chem. Phys. **100**, 4432 (1994).
[29]K. G. Kay, J. Chem. Phys. **100**, 4377 (1994).
[30]W. H. Miller, J. Chem. Phys. **53**, 1949 (1970).
[31]W. H. Miller, J. Chem. Phys. **53**, 3578 (1970).
[32]M. Church, S. V. Antipov, and N. Ananth, J. Chem. Phys. **146**, 234104 (2017).
[33]D. H. Zhang and E. Pollak, Phys. Rev. Lett. **93**, 140401 (2004).
[34]W. H. Miller, J. Phys. Chem. A **105**, 2942 (2001).
[35]K. G. Kay, Annu. Rev. Phys. Chem. **56**, 255 (2005).
[36]D. V. Shalashilin and M. S. Child, Chem. Phys. **304**, 103 (2004).
[37]L. Bonnet and J. Rayez, Chem. Phys. Lett. **277**, 183 (1997).
[38]L. Bonnet and J.-C. Rayez, Chem. Phys. Lett. **397**, 106 (2004).
[39]C. Crespos, J. Decock, P. Larregaray, and L. Bonnet, J. Phys. Chem. C **121**, 16854 (2017).
[40]B. Gu and S. Garashchuk, J. Phys. Chem. A **120**, 3023 (2016).
[41]S. Garashchuk, V. Rassolov, and O. Prezhdo, Rev. Comput. Chem. **27**, 287 (2011).
[42]R. Conte and E. Pollak, Phys. Rev. E **81**, 036704 (2010).
[43]R. Conte and E. Pollak, J. Chem. Phys. **136**, 094101 (2012).
[44]A. D. Kondorskiy and S. Nanbu, J. Chem. Phys. **143**, 114103 (2015).
[45]H. Nakamura, S. Nanbu, Y. Teranishi, and A. Ohta, Phys. Chem. Chem. Phys. **18**, 11972 (2016).
[46]S.-I. Koda, J. Chem. Phys. **143**, 244110 (2015).
[47]S.-I. Koda, J. Chem. Phys. **144**, 154108 (2016).
[48]C. T. Chapman and J. A. Cina, J. Chem. Phys. **127**, 114502 (2007).
[49]C. T. Chapman, X. Cheng, and J. A. Cina, J. Phys. Chem. A **115**, 3980 (2011).
[50]X. Cheng and J. A. Cina, J. Chem. Phys. **141**, 034113 (2014).
[51]F. Grossmann and A. L. Xavier, Phys. Lett. A **243**, 243 (1998).
[52]C. Harabati, J. M. Rost, and F. Grossmann, J. Chem. Phys. **120**, 26 (2004).
[53]F. Grossmann, Phys. Rev. A **60**, 1791 (1999).
[54]S. Bonella, D. Montemayor, and D. F. Coker, Proc. Natl. Acad. Sci. U. S. A. **102**, 6715 (2005).
[55]S. Bonella, G. Ciccotti, and R. Kapral, Chem. Phys. Lett. **484**, 399 (2010).
[56]F. Gottwald and S. D. Ivanov, e-print arXiv:1704.00477.
[57]W. H. Miller, Proc. Natl. Acad. Sci. U. S. A. **102**, 6660 (2005).
[58]M. Ceotto, G. F. Tantardini, and A. Aspuru-Guzik, J. Chem. Phys. **135**, 214108 (2011).
[59]M. Ceotto, S. Atahan, G. F. Tantardini, and A. Aspuru-Guzik, J. Chem. Phys. **130**, 234113 (2009).
[60]M. Ceotto, S. Atahan, S. Shim, G. F. Tantardini, and A. Aspuru-Guzik, Phys. Chem. Chem. Phys. **11**, 3861 (2009).
[61]M. Ceotto, D. Dell' Angelo, and G. F. Tantardini, J. Chem. Phys. **133**, 054701 (2010).
[62]R. Conte, A. Aspuru-Guzik, and M. Ceotto, J. Phys. Chem. Lett. **4**, 3407 (2013).
[63]F. Gabas, R. Conte, and M. Ceotto, J. Chem. Theory Comput. **13**, 2378 (2017).
[64]M. Ceotto, Y. Zhuang, and W. L. Hase, J. Chem. Phys. **138**, 054116 (2013).
[65]Y. Zhuang, M. R. Siebert, W. L. Hase, K. G. Kay, and M. Ceotto, J. Chem. Theory Comput. **9**, 54 (2012).
[66]B. J. Braams and J. M. Bowman, Int. Rev. Phys. Chem. **28**, 577 (2009).
[67]B. Jiang and H. Guo, J. Chem. Phys. **141**, 034109 (2014).
[68]R. Conte, C. Qu, and J. M. Bowman, J. Chem. Theory Comput. **11**, 1631 (2015).
[69]Z. Homayoon, R. Conte, C. Qu, and J. M. Bowman, J. Chem. Phys. **143**, 084302 (2015).
[70]Y. Paukku, K. R. Yang, Z. Varga, and D. G. Truhlar, J. Chem. Phys. **139**, 044309 (2013).
[71]R. Conte, P. L. Houston, and J. M. Bowman, J. Phys. Chem. A **119**, 12304 (2015).
[72]Z. Varga, R. Meana-Paneda, G. Song, Y. Paukku, and D. G. Truhlar, J. Chem. Phys. **144**, 024310 (2016).
[73]P. L. Houston, R. Conte, and J. M. Bowman, J. Phys. Chem. A **120**, 5103 (2016).
[74]R. Conte, B. Fu, E. Kamarchik, and J. M. Bowman, J. Chem. Phys. **139**, 044104 (2013).
[75]M. Ceotto, G. Di Liberto, and R. Conte, Phys. Rev. Lett. **119**, 010401 (2017).
[76]A. L. Kaledin and W. H. Miller, J. Chem. Phys. **118**, 7174 (2003).
[77]A. L. Kaledin and W. H. Miller, J. Chem. Phys. **119**, 3078 (2003).
[78]T. Halverson and B. Poirier, J. Phys. Chem. A **119**, 12417 (2015).
[79]R. P. Feynman and A. R. Hibbs, in *Quantum Mechanics and Path Integrals*, edited by R. P. Feynman and A. R. Hibbs (McGraw-Hill, 1965).
[80]M. V. Berry and K. Mount, Rep. Prog. Phys. **35**, 315 (1972).
[81]J. Liu and W. H. Miller, J. Chem. Phys. **127**, 114506 (2007).
[82]S. Takahashi and K. Takatsuka, J. Chem. Phys. **127**, 084112 (2007).
[83]G. Tao and W. H. Miller, J. Chem. Phys. **135**, 024104 (2011).
[84]J. H. Van Vleck, Proc. Natl. Acad. Sci. U. S. A. **14**, 178 (1928).
[85]M. C. Gutzwiller, J. Math. Phys. **8**, 1979 (1967).
[86]M. Baranger, M. A. de Aguiar, F. Keck, H.-J. Korsch, and B. Schellhaass, J. Phys. A **34**, 7227 (2001).
[87]M. Buchholz, F. Grossmann, and M. Ceotto, J. Chem. Phys. **144**, 094102 (2016).
[88]T. Yamamoto, H. Wang, and W. H. Miller, J. Chem. Phys. **116**, 7335 (2002).
[89]E. J. Heller, J. Chem. Phys. **75**, 2923 (1981).
[90]E. J. Heller, J. Chem. Phys. **94**, 2723 (1991).
[91]D. V. Shalashilin and M. S. Child, J. Chem. Phys. **115**, 5367 (2001).
[92]D. Tamascelli, F. S. Dambrosio, R. Conte, and M. Ceotto, J. Chem. Phys. **140**, 174109 (2014).
[93]G. Di Liberto and M. Ceotto, J. Chem. Phys. **145**, 144107 (2016).
[94]M. Ceotto, S. Valleau, G. F. Tantardini, and A. Aspuru-Guzik, J. Chem. Phys. **134**, 234103 (2011).
[95]K. Hinsen and G. R. Kneller, Mol. Simul. **23**, 275 (2000).
[96]B. B. Harland and P.-N. Roy, J. Chem. Phys. **118**, 4791 (2003).
[97]M. Wehrle, M. Šulc, and J. Vaníček, J. Chem. Phys. **140**, 244114 (2014).
[98]D. Picconi, F. J. A. Ferrer, R. Improta, A. Lami, and F. Santoro, Faraday Discuss. **163**, 223 (2013).
[99]L. S. Cederbaum, E. Gindensperger, and I. Burghardt, Phys. Rev. Lett. **94**, 113003 (2005).
[100]M. Wehrle, "Evaluation and analysis of vibrationally resolved electronic spectra with *ab initio* semiclassical dynamics," Ph.D. thesis, EPFL, 2015.
[101]D. T. Colbert and W. H. Miller, J. Chem. Phys. **96**, 1982 (1992).
[102]H. Partridge and D. W. Schwenke, J. Chem. Phys. **106**, 4618 (1997).
[103]J. Martin, T. J. Lee, and P. Taylor, J. Mol. Spectrosc. **160**, 105 (1993).
[104]S. Carter, N. Pinnavaia, and N. C. Handy, Chem. Phys. Lett. **240**, 400 (1995).
[105]T. J. Lee, J. M. Martin, and P. R. Taylor, J. Chem. Phys. **102**, 254 (1995).
[106]S. Carter, H. M. Shnider, and J. M. Bowman, J. Chem. Phys. **110**, 8417 (1999).
[107]O. Vendrell, F. Gatti, and H.-D. Meyer, J. Chem. Phys. **127**, 184303 (2007).

[108]M. Rossi, M. Ceriotti, and D. E. Manolopoulos, J. Chem. Phys. **140**, 234116 (2014).
[109]N. I. Hammer, E. G. Diken, J. R. Roscioli, M. A. Johnson, E. M. Myshakin, K. D. Jordan, A. B. McCoy, X. Huang, J. M. Bowman, and S. Carter, J. Chem. Phys. **122**, 244301 (2005).
[110]O. Vendrell, F. Gatti, and H.-D. Meyer, Angew. Chem., Int. Ed. **48**, 352 (2009).
[111]O. Vendrell, F. Gatti, and H.-D. Meyer, J. Chem. Phys. **131**, 034308 (2009).
[112]O. Vendrell, M. Brill, F. Gatti, D. Lauvergnat, and H.-D. Meyer, J. Chem. Phys. **130**, 234305 (2009).
[113]O. Vendrell, F. Gatti, and H.-D. Meyer, Angew. Chem., Int. Ed. **46**, 6918 (2007).
[114]O. Vendrell, F. Gatti, D. Lauvergnat, and H.-D. Meyer, J. Chem. Phys. **127**, 184302 (2007).
[115]O. Vendrell and H.-D. Meyer, Phys. Chem. Chem. Phys. **10**, 4692 (2008).
[116]A. B. McCoy, X. Huang, S. Carter, M. Y. Landeweer, and J. M. Bowman, "Full-dimensional vibrational calculations for $H_5O_2^+$ using an *ab initio* potential energy surface," J. Chem. Phys. **122**, 061101 (2005).
[117]X. Huang, B. J. Braams, and J. M. Bowman, J. Chem. Phys. **122**, 044308 (2005).
[118]S. Carter, J. M. Bowman, and A. R. Sharma, in *American Institute of Physics Conference Series* (American Institute of Physics, 2012), Vol. 1504, pp. 465–466.
[119]N. C. Handy, P. E. Maslen, R. D. Amos, J. S. Andrews, C. W. Murray, and G. J. Laming, Chem. Phys. Lett. **197**, 506 (1992).
[120]F. Grossmann, J. Chem. Phys. **125**, 014111 (2006).
[121]M. Buchholz, F. Grossmann, and M. Ceotto, J. Chem. Phys. **147**, 164110 (2017).